

Distinct electrider-like nature of infinite-layer nickelates and the resulting theoretical challenges to calculate their electronic structure

Kateryna Foyevtsova,^{1,2} Ilya Elfimov,^{1,2} and George A. Sawatzky^{1,2}

¹*Department of Physics & Astronomy, University of British Columbia, Vancouver, British Columbia V6T 1Z1, Canada*

²*Stewart Blusson Quantum Matter Institute, University of British Columbia, Vancouver, British Columbia V6T 1Z4, Canada*

(Dated: November 30, 2023)

We demonstrate in this paper that the recently discovered infinite-layer (IL) nickelates have much in common with a class of materials known as electrides. Oxide based electrides are compounds in which topotactic removal of loosely bound oxygens leaves behind voids with a landscape of attractive potentials for electrons. We show that this is also what happens in the IL nickelates, where one of the two electrons (per formula unit) freed during the topotactic synthesis is to a large degree located in the oxygen vacancy position, occupying partially a local s -symmetry interstitial orbital, rather than taking part alongside the other electron in converting Ni from 3+ to a full 1+ oxidation state. On the other hand, the involvement of the rare-earth $5d$ states is found to be rather indirect. Our study offers a new and detailed perspective on the mechanisms through which the presence of the interstitial charge can determine the superconducting and other properties of the IL nickelates. To this end, we demonstrate that the interstitial orbital in question, referred to by us as the zeronium s or $Z s$ orbital, forms strong covalent bonds with neighboring Ni $3d_{3z^2-r^2}$ orbitals, which in turn facilitates the one-dimensional-like dispersion of the Ni $3d_{3z^2-r^2}$ band along the c -axis direction, leading also to a possible large out-of-plane coupling between Ni magnetic moments. This finding, reinforced by our electron localization function analysis, points to a fundamental distinction between the nickelates and the structurally analogous cuprates, may explain the absence of superconductivity in hydrogen-poor samples, and is certainly in agreement with the observed large z -polarized component in the Ni L_3 -edge x-ray absorption spectra. In addition, by using DFT+U calculations as an illustration, we show that the electrider-like nature of the IL nickelates is one of the main reasons for the theoretical difficulty in determining the much debated elusive Fermi surface of these novel superconductors and also in exploring the possibility of them becoming excitonic insulators at low temperatures.

PACS numbers:

I. INTRODUCTION

The study of the recently discovered Ni-based high transition temperature (T_c) superconductors with an infinite-layer (IL) crystal structure¹⁻⁴ promises to provide important clues to our understanding of unconventional superconductivity in complex oxides. Such optimistic expectations are primarily fueled by the intriguing similarity that the nickelates bear with the famous superconducting cuprates^{5,6}. In both, the two-dimensional NiO₂ or CuO₂ layers constitute an essential part of the crystal structure [see Fig. 1 (a)], the transition metal (TM) ion is found in, formally, the same d^9 configuration, and a superconducting dome develops upon hole doping within similar doping ranges. As, however, intense research efforts rapidly expand our knowledge of the nickelate superconductors, important differences are becoming apparent, too (see reviews⁷⁻¹¹ and references therein). Thus, unlike the cuprates, the parent compounds of the IL nickelates behave as bad metals and, despite the evidenced strong short-range magnetic correlations¹²⁻¹⁵, seem to have a charge¹⁶ rather than spin¹³ ordered low-temperature state. Also, as the most recent experimental study reveals, superconductivity occurs only in samples with substantial hydrogen concentrations within a narrow range of 22 to 28 percent¹⁷.

These observations are in line with the conclusion from an early theoretical study of the nickelates' elec-

tronic structure¹⁸ that, notwithstanding their identical formal d electron count, “Ni⁺ is not Cu²⁺”, implying also a possibly different superconducting pairing mechanism. One of the major distinctions originates from the fact that the charge-transfer energy between the TM $3d$ and oxygen $2p$ states is considerably larger in the nickelates¹⁹, which, seemingly, justifies placing these systems in the Mott-Hubbard rather than charge-transfer regime of the Zaanen-Sawatzky-Allen (ZSA) classification scheme²⁰. Yet, a simple Ni $3d_{x^2-y^2}$ orbital based Mott-Hubbard picture is inconsistent with many of the key experimental features of the parent IL nickelates either. One obvious such feature is their metallic behavior that is likely to be related with the presence of two small electron pockets of mixed orbital characters, one at the Brillouin zone center and one at its corner, which are routinely seen in electronic structure calculations^{8,21}. It should be noted, though, that a full and precise determination of the nickelates' Fermi surface remains challenging to both theory and experiment. Also at odds with the single orbital scenario is the fact that the x-ray absorption spectra (XAS) at the Ni L_3 -edge have a strong z -polarized component, clearly indicating a presence of Ni $3d_{3z^2-r^2}$ holes in the ground state of the parent compounds²². Such observed partial occupation of the $3z^2 - r^2$ -symmetric Ni $3d$ orbital in addition to the $x^2 - y^2$ one makes it rather challenging to describe the IL nickelates using the ZSA classification scheme, since,

in order to keep the unit cell charge neutral, there must be electrons in formerly unoccupied states of local symmetry that can mix with the $3z^2 - r^2$ symmetry at the Ni site, which, however, are not provided by the atomic orbitals of the $R\text{NiO}_2$ crystal structure.

Given therefore that the IL nickelates seem to transcend the standard ZSA paradigm and also motivated by the recently suggested critical and intimately intertwined roles of the hydrogen and the interstitial charge for the nickelates' superconductivity, in this paper we take an alternative look at their electronic structure by considering the electrider concept frequently encountered in oxides prepared by a topotactic removal of selected oxygen ions^{23,24}. Scientific interest in electrider materials has recently been on a rise²⁵ and is driven by their exotic nature and a range of interesting physical properties they display, including superconductivity²⁶. Electriders consist of structural voids coordinated by mainly positive cations where unbound electrons resulting from the oxygen removal can get trapped by a strongly attractive potential. Rather than occupying the cation bands, these electrons are relatively localized in the voids and act like anions of charge -1 and spin $1/2$. An analogy with the IL nickelates can readily be drawn by considering the topotactic synthesis of the latter from the precursor rare-earth nickel perovskites $R\text{NiO}_3$ ($R = \text{La}, \text{Nd}, \text{or Pr}$), in which Ni ions assume a formal valence of $3+$. The extracted apical oxygens leave behind two electrons per formula unit which should, according to conventional thinking, convert Ni^{3+} into Ni^{1+} . However, it is quite feasible that whereas one of the two doped electrons is indeed on Ni, forming a very stable d^8 state with spin 1 as in NiO, the second electron is localized in the void at the O vacancy site which indeed is surrounded by four Nd^{3+} and two Ni ionic neighbors, with the actual ionic charges of the latter being closer to $2+$ than to $1+$ in our proposed electrider scenario.

In this paper, we use density functional theory (DFT) calculations to study the possibility of this actually occurring in NdNiO_2 , a representative parent IL nickelate, by explicitly introducing a fictitious atom without a nucleus at the oxygen vacancy site, which is represented by a large white sphere in Fig. 1 (a), and centering a set of basis functions around it. Without changing any physics, this allows us to analyze the electronic structure of NdNiO_2 in terms of local s , p , and d symmetries. We will call this fictitious atom “zeronium” because of its effective zero nuclear charge, a term coined in the late 1970s²⁷, and use a chemical symbol “Z” for it. We note that a variety of alternative terminologies exist. Thus, the electron occupying (either fully or partially) an interstitial orbital inside the void is also referred to in the literature as an interstitial, anionic, or electrider electron^{25,28} or as an interstitial quasiatom²⁹. As will be shown, the charge density of the Ni $d_{3z^2-r^2}$ character extends well into the interstitial region in the c direction, and by including Z we can quantify this in the same way that we can quantify the covalent mixing of the Ni $d_{x^2-y^2}$ orbital with the linear combination of the

neighboring O $2p$ orbitals of the $x^2 - y^2$ symmetry in the Zhang-Rice singlet³⁰. It will be emphasized that the hybridization between the Ni $d_{3z^2-r^2}$ and the Z s orbitals is by far more important in the interpretation of the low-energy electronic structure than the symmetry-restricted involvement of the Nd $5d$ and O $2p_\pi/2p_z$ states, which have been at the focus of most previous theoretical studies.

The structure of the paper is as follows. In Section II, we will describe our computational methods and provide details of our electronic structure calculations. In Section III, we will present our computational results, first demonstrating the importance of the hybridization between the zeronium s orbital and its two neighboring Ni $3d_{3z^2-r^2}$ orbitals along the c axis. The relatively secondary roles of the Nd $5d$ and O $2p_\pi/2p_z$ states will be illustrated by means of a computational experiment involving elimination of the Z s states from the vicinity of the Fermi level. We will then use the electron localization function (ELF) to show the real space localization of the electrider (*i.e.*, zeronium s) electron and compare NdNiO_2 with the iso-structural CaCuO_2 , finding the two of them to approach qualitatively very different electronic ground states in the limit of an exact-exchange (*i.e.*, Hartree-Fock) treatment. Further, we will show that the popular DFT+U method is seriously challenged in the presence of the strong covalent bonding between the zeronium s orbital and the Ni $3d_{3z^2-r^2}$ orbital, by highlighting qualitative inconsistencies between the results of DFT+U calculations obtained from different DFT codes. It will be emphasized that, since there is no doubt that these materials are strongly correlated, in the end it will be model Hamiltonians with methods like dynamical mean-field theory (DMFT) or exact diagonalization or impurity like approximations that are needed to describe the experimental data. In Section IV, drawing support from our computational results and from the recent impurity calculations by Jiang *et al.*³¹, we will discuss a realistic electronic configuration for Ni in the parent IL nickelates, in which the zeronium states play one of the key roles giving rise to such strongly contributing configurations as $d_{x^2-y^2, z^2}^{8, S=1} s$ and $d_{z^2}^9 \underline{L}_{x^2-y^2} s$, where s denotes an electron in Z s and \underline{L} a hole in O $2p$. This will be followed by a short discussion of the possibility for the nickelates to transition into an excitonic insulating state at low temperatures. Conclusions will be offered in Section V.

II. METHODS

We consider primitive unit cells of NdNiO_2 , with the lattice constants $a = 3.91 \text{ \AA}$ and $c = 3.37 \text{ \AA}$, and of CaCuO_2 , with the lattice constants $a = 3.86 \text{ \AA}$ and $c = 3.20 \text{ \AA}$. When not specified otherwise, our DFT calculations are performed using the augmented plane wave all-electron package WIEN2k³² and choosing the gradient-corrected local density approximation

(GGA)³³ for the energy functional to treat the exchange and correlation effects. We use $RK_{\max} = 7.0$ and a $12 \times 12 \times 14$ Γ -centered k -point grid for bandstructure calculations but increase the RK_{\max} value to 9.0 for calculating ELF. The atomic muffin-tin radii R are set as $R(\text{Nd})=2.5$, $R(\text{Ni})=1.57$, $R(\text{O})=2.12$, and $R(\text{Z})=1.61$ in bohr [$R(\text{Nd})=1.32$, $R(\text{Ni})=0.83$, $R(\text{O})=1.12$, and $R(\text{Z})=0.85$ in Å]. The three Nd $4f$ electrons are treated as core electrons. For the two-formula-unit supercell with the G -type ordering of Ni spins considered in Section III C, we use a $10 \times 10 \times 10$ Γ -centered k -point grid and keep the same values for $RK_{\max} = 7.0$ and for the muffin-tin radii. We find that it is important to use the tetrahedron rather than smearing method for integrating over the Brillouin zone³⁴, since otherwise the Fermi level can be determined incorrectly resulting in a loss of the hole Fermi pockets, which would obviously violate the charge neutrality principle.

In addition to WIEN2k, two pseudo-potential codes, VASP³⁵ and Quantum Espresso^{36,37}, are also used in order to calculate the ELF of NdNiO₂ and CaCuO₂ within the hybrid functional method and/or the Fermi surface of NdNiO₂ within the DFT+U method. In these calculations, the energy cut-offs are set to ENCUT=320 eV and ecutwfc=60 Ry in VASP and Quantum Espresso, respectively. In the case of hybrid functional calculations on the primitive unit cells of NdNiO₂ and CaCuO₂, the size of the k -point grid is reduced down to $6 \times 6 \times 6$.

The Wannier functions based analysis of the bandstructure of NdNiO₂ is performed by using the maximally localized Wannier functions (MLWF) method³⁸ as implemented in the WANNIER90 code³⁹.

III. RESULTS

A. Zeronium s orbital without magnetism and correlations

In Figs. 1 (b) and (c) we present a typical result of a non-spin-polarized GGA calculation on NdNiO₂, in a form of atomic orbital projected band dispersion diagrams. This should give us information about the directional dependence of the dispersion of the various atomic like states, which is the first step in the evolution of a model Hamiltonian approach to the problem. As already mentioned, two electron pocket bands cross the Fermi level beside the cuprate-like $3d_{x^2-y^2}$ band, one with a strong Nd $5d_{3z^2-r^2}$ character at Γ and one with mixed Nd $5d_{xy}$ and Ni $3d_{3z^2-r^2}$ characters at A . Most interesting, though, is the fact that the Ni $3d_{3z^2-r^2}$ states are found to behave in a rather non-trivial way⁴⁰. Thus, while along the $Z-R-A-Z$ k -path, which belongs to the $k_z = \pi$ Brillouin zone boundary, the Ni $3d_{3z^2-r^2}$ band is flat and lies fully below the Fermi level at around -1 eV, it then strongly disperses along the c direction going from Z to Γ where it stops at around -3 eV and roughly stays there in the entire $k_z = 0$ plane (the $\Gamma-X-M-\Gamma$

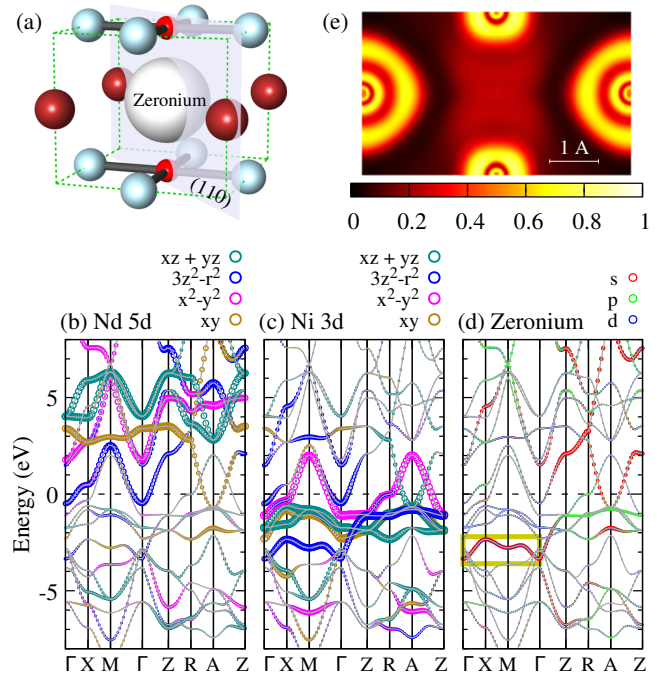


FIG. 1: (a) Crystal structure of infinite-layer nickelates $R\text{NiO}_2$ (R =rare-earth atom). Different atoms are represented by spheres as follows: R = large red, Ni = small red, O = blue, O vacancy (zeronium) = large white at the center of the unit cell. (b) and (c) Band structure of NdNiO₂ from a non-spin-polarized GGA calculation projected onto atomic (b) Nd $5d$ and (c) Ni $3d$ orbitals. Orbital character in a given state is proportional to the area of a respective color. (d) Same NdNiO₂ band structure as in (c) and (b) but projected onto the zeronium orbitals with s , p , and d symmetries. The yellow rectangle highlights the bonding combination of the Ni $3d_{3z^2-r^2}$ and Z s orbitals at k -vectors with $k_z = 0$. The zero of energy is at the Fermi energy. (e) Electron localization function (ELF) of NdNiO₂ in the (110) plane crossing Nd, Ni, and oxygen vacancy sites as shown in (a).

sector). Moreover, at all the k -vectors with $k_z \neq \pi$ the Ni $3d_{3z^2-r^2}$ states become scattered over multiple bands in a wide energy range both below and above the Fermi level, which signals their partial occupation and ensuing active involvement in low-energy electronic excitations.

The near flat band behaviour in the variation of the in-plane k for $k_z = 0$ or $k_z = \pi$ suggests that the band has a strong one-dimensional (1D) character. Remarkably, it becomes clear from inspecting the zeronium local orbital projections in Fig. 1 (d) that such 1D like behaviour is a result of the strong mixing of the Ni $3d_{3z^2-r^2}$ states with the interstitial states in the c axis direction. Indeed, one finds that, on one hand, the zeronium s orbital has a large contribution to the occupied band at around -3 eV, which is highlighted by a yellow rectangle in the figure, at k -points with $k_z = 0$ (the $\Gamma-X-M-\Gamma$ sector). This is also the band that has a strong Ni $3d_{3z^2-r^2}$ character in Fig. 1 (c). On the other hand, at the k -points with

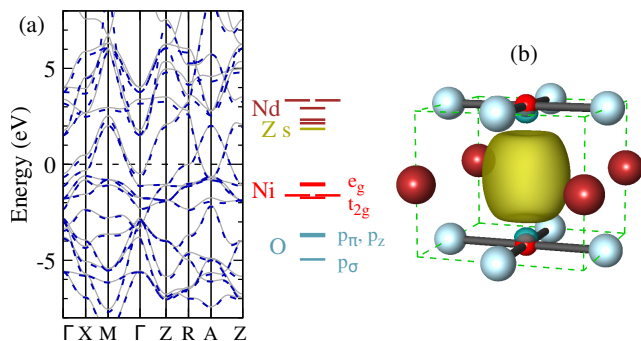


FIG. 2: (a) GGA (solid grey) and TB model (dashed blue) band dispersions of NdNiO₂. On the right-hand side also shown is the energy-level diagram with the on-site energies of the 17 atomic and electronegative orbitals entering our TB model. The Fermi energy is at zero. (b) The zeronium s Wannier function.

$k_z = \pi$ (the $Z-R-A-Z$ sector), the $Z s$ orbital character is mostly above the Fermi level, while the Ni $3d_{3z^2-r^2}$ orbital character is fully concentrated in the occupied band at around -1 eV. This is consistent with the fact that, by symmetry, an s orbital and a $3z^2 - r^2$ orbital that alternate along the z direction have the strongest coupling when $k_z = 0$ and zero coupling when $k_z = \pi$. Hence, the band at -3 eV enclosed in the yellow rectangle corresponds to the bonding combination of the Ni $3d_{3z^2-r^2}$ and $Z s$ orbitals, whereas their anti-bonding combination is pushed above the Fermi level where it hybridizes with empty Nd $5d$ orbitals. This also explains why in the $Z-R-A-Z$ sector the Ni $3d_{3z^2-r^2}$ band at -1 eV appears flat and well disentangled from other bands, because this is where $k_z = \pi$ and its coupling with the $Z s$ states is canceled out. Moreover, because of the large radial extent of the Ni $3d_{3z^2-r^2}$ orbital in the z directions and small extent in the plane, the hybridization in the in-plane directions will be relatively small. Note that coupling of $Z s$ to any of the other four Ni $3d$ orbitals is symmetry forbidden at any k -vector. As shown in Supplementary Material⁴¹, very similar band structures with the same zeronium features are obtained for PrNiO₂⁴² and LaNiO₂⁴³, two other parent IL nickelates demonstrating superconductivity upon doping.

We also perform an MLWF analysis of the NdNiO₂ bandstructure using the five Nd $5d$ orbitals, the five Ni $3d$ orbitals, the three $2p$ orbitals of each one of the two oxygens in the primitive unit cell, and the $Z s$ orbital as a basis of the corresponding effective tight-binding (TB) model. We note that several other studies have been reported that also consider an empty s -symmetry interstitial orbital centered at the O vacancy sites^{17,44-46} but here we focus on discussing the important ways it plays a role in the physical interpretation of the band structure of NdNiO₂ and especially of the unusual dispersion of the Ni $3d_{3z^2-r^2}$ band. The quality of the agreement

TABLE I: The on-site energies in eV of the 17 orbitals entering our MLWF based TB model. The Fermi energy is at zero.

		Z s 1.84	
		Ni	Nd
$3d_{xy}$	-1.74	$5d_{xy}$	2.15
$3d_{xz,yz}$	-1.61	$5d_{xz,yz}$	3.34
$3d_{x^2-y^2}$	-1.01	$5d_{x^2-y^2}$	2.93
$3d_{3z^2-r^2}$	-1.08	$5d_{3z^2-r^2}$	2.33
		O	
		$2p_\sigma$	-4.96
		$2p_\pi$	-3.74
		$2p_z$	-3.64

between our TB model's and the GGA energy bands is very good, as one can see in Fig. 2 (a). Figure 2 (b) shows the $Z s$ Wannier function in real space, and Tables I and II provide the on-site energies and the largest nearest-neighbor hopping integrals in the model. These parameter values can be used in model Hamiltonians by transforming them into a configuration interactions like picture and adding in the on-site Coulomb and exchange interactions as done in the recent study by Jiang *et al.*³¹. As one can see in Tables I and II, the on-site energies of the Ni $3d_{3z^2-r^2}$ and $Z s$ orbitals are -1.08 eV and 1.84 eV, respectively, and the nearest-neighbor electron hopping integral between them is -1.14 eV, which is almost as large as the $dp\sigma$ hopping of 1.32 eV between the Ni $3d_{x^2-y^2}$ and O $2p_\sigma$ orbitals. Interesting also is that the on-site energies of the Nd $5d$ orbitals are all higher than that of the $Z s$ orbital, as we also demonstrate in the energy-level diagram of Fig. 2 (a). The hybridization of the $Z s$ orbital with the Nd $5d_{xy}$ states at higher energies pushes the bonding part down and it is this that causes the highly mixed band crossing the Fermi energy and forming the electron pocket at A .

It is important to discuss the large nearest-neighbor $Z s$ -Ni $3d_{3z^2-r^2}$ hopping in the light of the recent hydrogen experiments¹⁷ that indicate that superconductivity in the Sr substituted NdNiO₂ is only present if there is a substantial amount of H in the structure. As other theoretical studies have shown⁴⁷, that hydrogen assumes a close to H^- ionic state and favours to be in the O vacancy position. If this is correct, then we note that the presence of H^- would block the $Z s$ -Ni $3d_{3z^2-r^2}$ hybridization since the vacancy position is already occupied by a negative charge. This would put the Ni electronic structure close to that of Cu in the cuprates. One could also speculate that the inclusion of some F^- in the vacancy position could do the same and perhaps more efficiently. This is worth a try but one should also realize that the

TABLE II: The nearest-neighbor electron hopping integrals in eV in our MLWF based TB model. Only those with the absolute values larger than 0.3 eV are listed. The σ and π designations of the O $2p$ orbitals are done considering their position relative to a neighboring Ni atom. Note that there is no Nd $5d$ –Ni $3d$ hybridization in this list, which indicates that the dominant interaction path between these two orbitals is through Z s .

Z s –Ni $3d_{3z^2-r^2}$	-1.14	Ni $3d_{x^2-y^2}$ –O $2p_\sigma$	1.32
Z s –Nd $5d_{xy}$	-1.04	Ni $3d_{3z^2-r^2}$ –Z s	-1.14
Z s –Nd $5d_{3z^2-r^2}$	0.66	Ni $3d_{xz}$ –O $2p_z$	0.78
Z s –O $2p_\sigma$	0.66	Ni $3d_{xy}$ –O $2p_\pi$	0.71
Z s –O $2p_z$	0.65	Ni $3d_{3z^2-r^2}$ –O $2p_\sigma$	0.67
Nd $5d_{xz,yz}$ –O $2p_\pi$	1.22	O $2p_\sigma$ –O $2p_\sigma$	0.40
Nd $5d_{xy}$ –Z s	-1.04	O $2p_\pi$ –O $2p_\pi$	-0.36
Nd $5d_{xz,yz}$ –O $2p_z$	0.96		
Nd $5d_{x^2-y^2}$ –O $2p_z$	0.88		
Nd $5d_{xy}$ –O $2p_\sigma$	0.56		
Nd $5d_{3z^2-r^2}$ –O $2p_\pi$	0.53		
Nd $5d_{xz,yz}$ –O $2p_\sigma$	0.50		
Nd $5d_{x^2-y^2}$ –O $2p_\pi$	0.41		
Nd $5d_{3z^2-r^2}$ –O $2p_z$	-0.32		

relatively large size of F^- could cause a substantial c axis expansion which may indeed act to destabilize the structure.

B. Computational experiment

In contrast with the emphasis on the Nd $5d$ states that prevails in the literature, our results from Table II indicate that their direct hybridization with the Ni $3d_{3z^2-r^2}$ and Ni $3d_{x^2-y^2}$ orbitals is small, but it is rather the Z s orbital that mediates the involvement of these empty states with the Ni states.

To better illustrate this important observation, we consider here results from a computational experiment where the Z s orbital is intentionally removed from playing any role in the low-energy electronic properties. This can be achieved via a charge self-consistent calculation where electrons are made to pay a high energy cost for occupying this orbital. The resulting bandstructure shown in Figs. 3 (a) and (b) displays significant differences with the original one in Figs. 1 (b) and (c). Most notably, the Ni $3d_{3z^2-r^2}$ band becomes essentially flat throughout the entire Brillouin zone. Its dramatic transformation is emphasized in Fig. 3 (c) showing the Ni $3d_{3z^2-r^2}$ projected

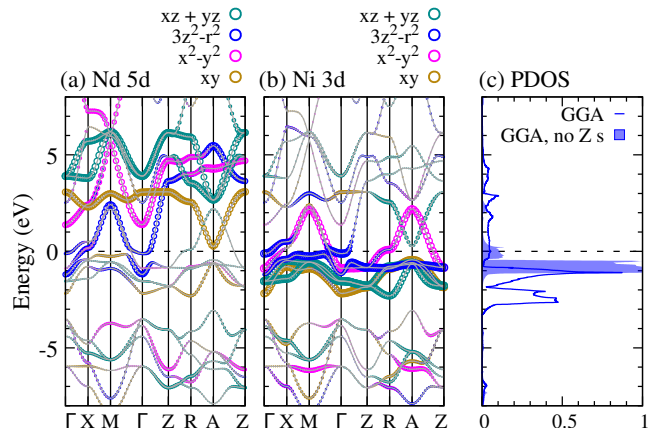


FIG. 3: The result of a computational experiment where the zeronium s orbital is forcefully depopulated yielding significant changes in the NdNiO₂ electronic structure around the Fermi level: (a) and (b) Atomic orbital projections of the altered band structure. (c) A comparison between the Ni $3d_{3z^2-r^2}$ projected densities of states (PDOS) of NdNiO₂ before (“GGA”) and after (“GGA, no Z s ”) depopulating the Z s orbital. The Fermi energy is at zero.

densities of states before and after the removal of the Z s orbital. Furthermore, instead of two electron pocket bands, we now have only one at Γ , of mainly Nd $5d_{3z^2-r^2}$ character. It crosses and hybridizes with the Ni $3d_{3z^2-r^2}$ band, but this hybridization is much weaker compared to that between the Ni $3d_{3z^2-r^2}$ and Z s bands, in accordance with Table II. In essence, the Ni $3d_{3z^2-r^2}$ orbital becomes much more atomic-like here, while it clearly cannot be treated as such in reality because of its strong covalent bonding with the zeronium s orbital.

C. ELF (electron localization function)

We find a total of 0.36 electrone electrons inside a sphere of radius 0.85 Å around the vacancy site, out of which 0.24 occupy the local s orbital. This is large enough to support the electrone scenario, but (as it is often the case in studies on electrines²⁸) not sufficient to produce a significantly visible maximum in the real-space electron density distribution, due to the strong background density of other electrons. There is, however, a better way of measuring electron localization in an electrone material which is by using the electron localization function (ELF)^{48,49}. ELF has been established as one of the best descriptors for identifying electrone systems²⁸. The definition of ELF is tailored such that its value can vary between 0 and 1, with 1 corresponding to maximal electron localization. As one can see in Fig. 1 (e), the computed ELF of NdNiO₂ has a clear maximum at the oxygen vacancy (*i. e.*, zeronium) site. A maximum of a similar strength was taken as a sign of an electrone-like nature of the prototypical electrone

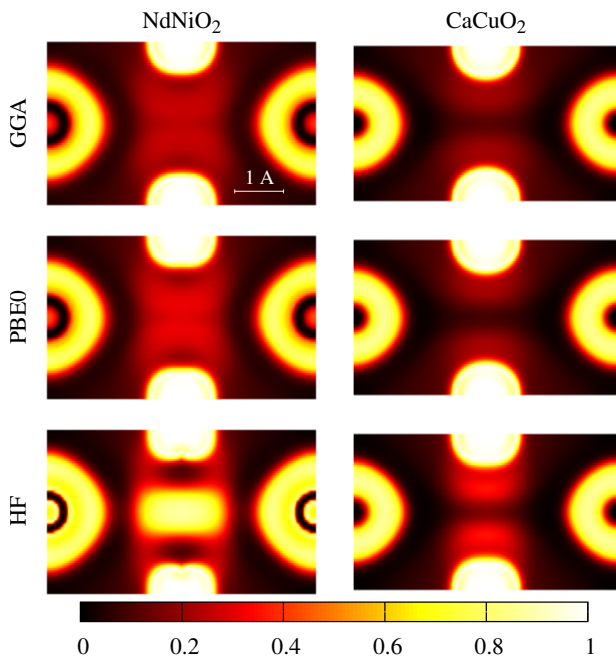


FIG. 4: Electron localization functions of NdNiO_2 and CaCuO_2 in the (110) crystal plane, calculated using the GGA, PBE0, and Hartree-Fock (HF) methods and the pseudo-potential code Quantum Espresso.

compound $[\text{Ca}_{24}\text{Al}_{28}\text{O}_{64}]^{4+}(4e^-)^{24}$.

There is also a clear minimum in the ELF of NdNiO_2 at a distance of about 1 Å going from the Ni site towards the Z site. This further indicates that the electron density in that region cannot be derived solely from the Ni 3d wave function but rather from a combination of the Ni 3d and Z s wave functions, because a pure atomic 3d wave function does not have a radial node. An alternative interpretation would be to say that this minimum is a result of an effective mixing of the Ni 3d states with the 4d states, a point of view adopted, for instance, by Katukuri *et al.* in Ref. 50. The 4d wave function of an isolated Ni^+ ion has its node indeed close to 1 Å from the Ni nucleus. This observation is of great importance in the development of model Hamiltonians to describe these correlated electron systems and, as we will argue below, might also help us understand better the results of DFT+U calculations.

It is interesting to compare the ELF of NdNiO_2 with that of the iso-structural cuprate system CaCuO_2 . The two top panels of Fig. 4 show their ELFs obtained from ferromagnetically spin-polarized GGA calculations using the pseudo-potential code Quantum Espresso. We will explain the need to switch to both a new code and a new magnetic configuration below, but for now let us note that this does not change the ELFs of the considered oxides in the region around the zeronium, as one can see by comparing with Fig. 1 (e). An important result is that, opposite to NdNiO_2 , the ELF of CaCuO_2 has a

minimum rather than a maximum at the oxygen vacancy site. This indicates that the electrone-like electronic behavior of the IL nickelates is a unique feature that makes them distinctly different from the cuprates.

Moreover, this difference becomes more and more pronounced as one switches to using a hybrid functional with some amount of an exact [*i. e.*, Hartree-Fock (HF)] exchange in it, a strategy known to help improve the description of electronic correlations and electron localization, particularly, in the case of electrone electrons (see Ref. 28, page 9373). We consider the PBE0 hybrid functional method⁵¹ which is based on the following simple expression for the exchange ("x") and correlation ("c") energy functional:

$$E_{\text{xc}}^{\text{PBE0}} = \frac{1}{4}E_{\text{x}}^{\text{HF}} + \frac{3}{4}E_{\text{x}}^{\text{GGA}} + E_{\text{c}}^{\text{GGA}},$$

in which a quarter of the exchange term of the original GGA functional is proportionally replaced by an HF contribution. As one can see in the two middle panels of Fig. 4, introducing a quarter of an exact exchange results in an enhanced localization of the electrone electron in NdNiO_2 but does little in the case of CaCuO_2 , which reinforces our previously stated conclusions. Finally, performing a pure HF calculation (the bottom panels of Fig. 4) is found to drive the electrone electron of NdNiO_2 towards full localization.

Before finishing this section, let us explain our choices regarding the magnetic configuration and the DFT code used to produce the results in Fig. 4. First, it becomes very challenging to stabilize a non-magnetic solution as soon as one adds some amount of an exact exchange into the energy functional, and therefore all the calculations presented in Fig. 4 are performed keeping consistently the same ferromagnetically ordered Ni spin configuration, which is the only possible configuration one can have in a primitive unit cell. Second, in the case of hybrid functional calculations, computational efficiency becomes a serious issue which can be better dealt with in a pseudo-potential code like Quantum Espresso. For the same reason, we did not choose to consider here some kind of an antiferromagnetic order, as this would require using a computationally more demanding multiple formula unit supercell.

D. Can one use the DFT+U method to unveil the Fermi surface of the IL nickelates?

We now explore further how magnetism and electronic correlations might affect the behavior of the electrone electrons in the parent IL nickelates. Our hybrid functional calculations already indicate that correlations can strongly enhance their electrone-like properties, but a detailed study would require us to use a more computationally flexible method. Therefore, we will consider here the popular DFT+U approximation⁵², in which local electronic correlation effects are treated in a static mean-field fashion. This is a method that has extensively been

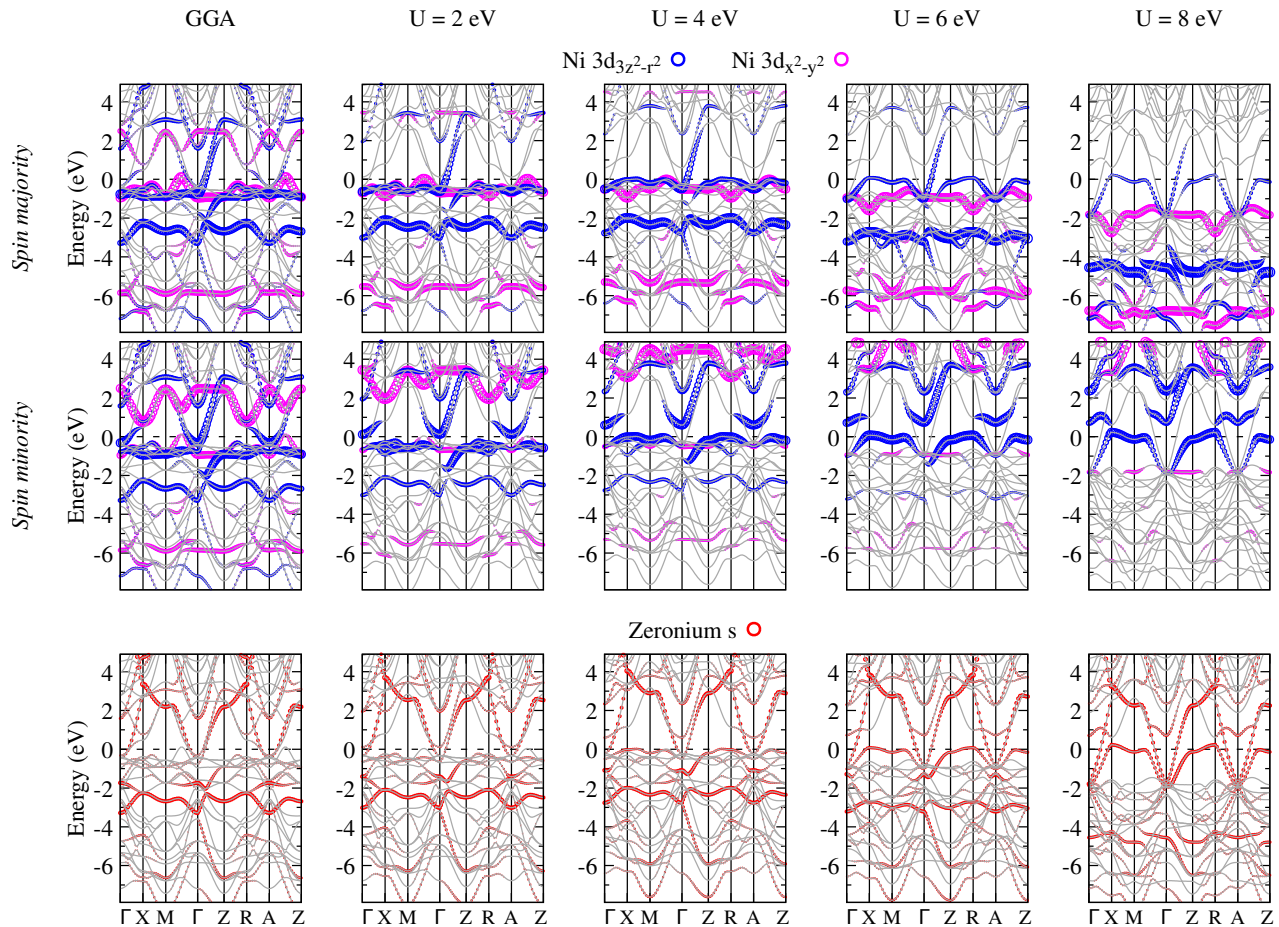


FIG. 5: The band structure of NdNiO_2 in the G -type antiferromagnetically ordered state obtained from WIEN2k with Ni atomic and electrone orbital projections as a function of U in the DFT+ U method. The Fermi energy is at zero.

used in computational studies of various TM compounds with strong on-site electronic correlations, including the IL nickelates^{21,53,54}. Its efficiency, however, comes at a price. First, with DFT+ U one is bound to deal with a magnetically long-range ordered state, which is different from the experimentally observed ground state of the parent IL nickelates where localized magnetic moments, although indeed present, have no long-range correlations¹². Second, in DFT+ U the electron interaction parameters appear as adjustable parameters, introducing additional uncertainty. There are also other, more subtle yet potentially very important, differences in how a DFT+ U calculation can be set up, which will be discussed later.

Figure 5 shows the evolution of the DFT+ U band structure of NdNiO_2 as a function of U , the on-site Coulomb repulsion between Ni $3d$ electrons. The Hund's rule exchange coupling, J_H , is set to zero for simplicity. We note, however, that this does not mean that the net J_H is zero, because in DFT full exchange is included already at the GGA level but with a Hamiltonian involving only $S_z \cdot S_z$ terms. In other words, the Hund's rule exchange is treated as Ising-like since DFT methods with \vec{k}

as a good quantum number have only S_z and not the local S as a good quantum number. This is very important since the singlet energy in $J\vec{S} \cdot \vec{S}$ is $-3/4J$ for spin 1/2 and the triplet energy is $+1/4J$, while for the Ising-like interaction the spin parallel and antiparallel energies are $\mp 1/4J$.

We order the Ni spin magnetic moments antiferromagnetically with a $Q = (\pi, \pi, \pi)$ (*i. e.*, G -type) ordering vector, which causes doubling of the unit cell and, consequently, of the number of bands compared with Figs. 1 (b)-(d). As mentioned earlier, the need to have a long-range magnetic order is an unavoidable component of DFT+ U , reflecting the static nature of this approach. However, as for example discussed by Trimarchi and co-workers⁵⁵, the influence of the kind of magnetic order usually is very small especially if there are resulting strongly localized spins in the ordered state.

Several comments are to be made regarding the antiferromagnetic GGA results presented in the left-most column of Fig. 5. First, like in the cuprates, spin polarization occurs involving mainly the Ni $3d_{x^2-y^2}$ bands. Second, this has almost no effect on the Z s bands, in-

cluding the occupied ones at -3 eV, which means that the electrone-like nature of the compound stays intact. The small electron pockets at Γ and A (now folded on top of each other) are also preserved. But now, because of the antiferromagnetic splitting of the Ni $3d_{x^2-y^2}$ bands, the compensating positive charge is located in the similarly small hole pockets at half way between M and Γ (and, equivalently, A and Z) and has a spin majority Ni $3d_{x^2-y^2}$ orbital character. This suggests that, within the rigid band shift approximation, in the chemically hole-doped superconducting nickelates like $\text{Sr}_x\text{Nd}_{1-x}\text{NiO}_2$, doped holes should bind with the stoichiometric holes into local singlets with the $x^2 - y^2$ symmetry, a situation similar to what happens in the cuprates^{19,31}. Note that the occupied $x^2 - y^2$ states are strongly hybridized with the same symmetry molecular combination of O $2p$ orbitals as in the Zhang-Rice picture, which is obvious from the $x^2 - y^2$ symmetry states forming another band at between 5 and 6 eV of mainly O $2p$ molecular orbital character.

This picture, however, changes into a qualitatively very different one as the value of U starts to increase. First, the Ni $3d_{3z^2-r^2}$ electrons become spin-polarized too and get coupled ferromagnetically with the Ni $3d_{x^2-y^2}$ electrons. Second, only one electron pocket survives. Also, instead of the spin *majority* Ni $3d_{x^2-y^2}$ hole pocket between M and Γ , we have now for $U > 4$ eV a shallow hole pocket at X (and, equivalently, R) with a spin *minority* Ni $3d_{3z^2-r^2}$ orbital character. In this situation, the chemically doped holes and the stoichiometric holes would be found forming local triplets rather than singlets, which could possibly lead to a superconducting state with a completely different symmetry and perhaps even of a fundamentally different nature. Interestingly, the Z s orbital will play an important role in this scenario as at large U it acquires a substantial weight in the hole pocket band at X resulting from its strong hybridization with the Ni $3d_{3z^2-r^2}$ orbital.

We have noticed that some of the published DFT+U based studies^{21,53,54} of the IL nickelates report a qualitatively different U -dependence of the electronic structure, finding in particular that there is a charge gap opening at $U = 8$ eV, whereas in our DFT+U calculations NdNiO_2 remains metallic at all U . Suspecting that the difference in the choice of a DFT code might be the issue, we repeat our calculations using also the pseudo-potential codes VASP and Quantum Espresso. The obtained results as a function of U and a DFT code are summarized in Fig. 6 in a form of Fermi surfaces. Indeed, the three considered DFT codes are found to give qualitatively different U -dependence for the Fermi surface of NdNiO_2 and, as such, for its electronic structure overall.

We stress that within each code we have intentionally chosen to use *nominally* the same rotationally invariant formulation of the DFT+U method by Liechtenstein *et al.*⁵⁶ (which is often referred to as a "self-interaction correction" method). Therefore, the main source for the discrepancy has to be the different ways that the codes use

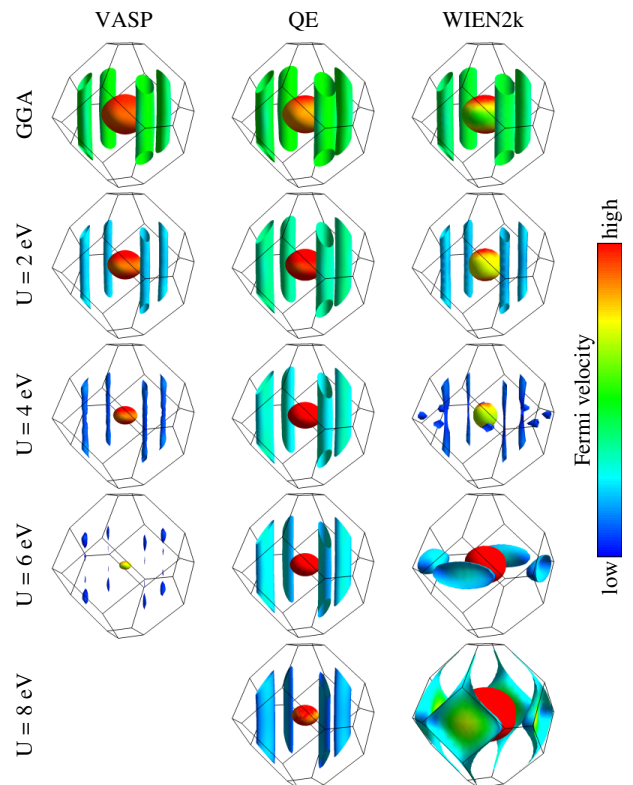


FIG. 6: Fermi surface of NdNiO_2 calculated in DFT+U using different DFT codes for a range of on-site Hubbard interaction parameters $U = 0, 2, 4, 6,$ and 8 eV. The Hund's exchange coupling is set to zero. The Fermi surface color represents the Fermi velocity.

to define local Ni $3d$ orbitals for calculating occupation matrices in DFT+U expressions. By default, atomic and Lowdin orthogonalized atomic wave functions are used in QE and VASP, respectively, whereas WIEN2k considers atomic-like wave functions that go to zero outside muffin tin spheres. These differences have minor effect when the correlated orbitals in question are well-localized (see, for instance, corresponding results for CaCuO_2 in Supplementary Material⁴¹), but become critically important in the presence of strong hybridization with uncorrelated subset. In the case of the IL nickelates, such is primarily the hybridization between the Ni $3d_{3z^2-r^2}$ and Z s orbitals. One way to see this is by noticing that it is the hole pocket band of exactly that mixed Ni $3d_{3z^2-r^2}$ and Z s orbital character that gets pinned to the Fermi level at $U > 4$ eV in WIEN2k and whose absence results in the charge gap opening in VASP. This strong hybridization is all but absent in the cuprates, while both have relatively strong hybridization of the O $2p$ and the TM $3d_{x^2-y^2}$ orbitals although weaker for the nickelates because of the larger charge-transfer energy.

It is also worth mentioning that in WIEN2k projections onto local states of a certain symmetry are done without considering the radial dependence, *i. e.*, with-

out differentiating between principal quantum numbers, while in VASP and Quantum Espresso this is not the case, which, in the light of our earlier argument about the possible mixing of Ni $3d$ and $4d$ states, can be another important factor contributing to the discrepancy.

Summarizing this section, Fig. 6 provides yet another demonstration of the important role of the Z s orbital coupled with the Ni $3d_{3z^2-r^2}$ orbital in a strong covalent bond. Such unique property of the IL nickelates combined with the discussed limitations of the DFT+U method causes an uncertainty in the nature of the symmetry of the hole pocket and the states that are closest to the Fermi level.

IV. DISCUSSION

A. Ni electronic configuration: d^9 , d^8s , or $d^9s\bar{L}$?

Our presented DFT based analysis of the parent IL nickelates points to a microscopic picture where the oxygen vacancy centered s orbital hybridizes very strongly with the Ni $3d_{3z^2-r^2}$ orbital, pulling a large portion of its atomic electron density into the interstitial region. As a result, these two orbitals form a bonding and an anti-bonding states, with the bonding state having larger Ni $3d$ than Z s character and being totally occupied and with the anti-bonding state having more Z s character and being totally empty. This leads to a substantial hole concentration in the Ni $3d_{3z^2-r^2}$ band driving Ni^+ towards Ni^{2+} . Noteworthily, a series of recent DFT+DMFT studies have arrived at a similar conclusion about the Ni ionisation state^{46,57-65}. Such deviation from the nominal valency is reminiscent of that encountered in negative charge-transfer compounds^{20,66}, but here the role of ligand states pulling in holes from the transition metal states is delegated to the zeronium s states pulling in electrons. Many materials with rich physics belong to this class, including the high- T_c superconductors bismuth oxides^{67,68}, the battery material LiNiO_2 with a proposed electronic high-entropy state^{69,70}, and also the previously mentioned precursor compounds $R\text{NiO}_3$ ⁷¹. In $R\text{NiO}_3$, for instance, a negative value of the charge-transfer energy between the Ni $3d$ and O $2p$ states is known to result in a $d^8\bar{L}$ (Ni^{2+}) rather than the formal d^7 (Ni^{3+}) configuration for Ni ions, where \bar{L} stands for an O $2p$ hole coupled strongly in a covalent bond with a Ni $3d$ hole. By analogy, we can say that in the IL nickelates a state like d^8s , with s denoting an electron in the Z s orbital bound in a strong covalent bond with neighboring Ni $3d_{3z^2-r^2}$ orbitals, should have a substantial weight in the ground state Ni configuration.

It is important to keep in mind that in order to fully reveal the true ground state configuration of Ni, including the local spin and multiplet structure, one needs to go beyond DFT and use advanced many-body techniques. In this regard, recent configuration interaction based impurity calculations by Jiang *et al.*³¹ show that the ground

state is a mixture of similarly strong contributions from the $d_{x^2-y^2}^9$, $d_{x^2-y^2, z^2}^{8, S=1}$ s , $d_{z^2}^9 \bar{L}_{x^2-y^2}$ s , and $d^{10} \bar{L}_{x^2-y^2}$ configurations, all having a net spin of $1/2$. This is very different from the cuprates where the ground state electronic structure is dominated by $d_{x^2-y^2}^9$ and $d^{10} \bar{L}_{x^2-y^2}$.

Our findings complement the ideas from Ref. 17 about the possibility of the interstitial charge suppressing superconductivity in hydrogen-poor samples. We emphasize, however, that it is the nearest-neighbor Z s -Ni $3d_{3z^2-r^2}$ hybridization that is primarily responsible for turning the stoichiometric nickelates into effectively three-dimensional systems and thus driving them away from the two-dimensional regime that is known to favor superconductivity in cuprates. This is supported by the calculations for the 20 percent hole doped LaNiO_2 system presented in Supplementary Material⁴¹, in which the electrone-like nature and the associated strong out-of-plane electronic coupling are found to be well preserved.

Important implications regarding magnetism are also in place. The on-site Hund's rule coupling dictates that the Ni $3d_{3z^2-r^2}$ holes have the same spin as the $d_{x^2-y^2}$ holes, again pointing to a strong admixture of the d^8 ($S=1$) state in the net ground state configuration of Ni. This is indeed what our DFT+U calculations in Fig. 5 suggest and what the mentioned DFT+DMFT studies report and is in line with the conclusions of the impurity calculations including all multiplets by Jiang *et al.*³¹ We can also think of this as a large part of the $\text{Ni}^+ 3d_{3z^2-r^2}$ electron finding itself in the zeronium site with spin parallel to the local $d_{x^2-y^2}$ remaining electron. This would result in a very strong anti-ferromagnetic coupling between the Ni spins in the one-dimensional chains along the c direction, whose consequences require a detailed theoretical exploration, especially, in connection with the low-energy excitations seen in the recent resonant inelastic x-ray scattering (RIXS) experiments^{15,22}, but this kind of a study is beyond the scope of the present work.

B. Possible excitonic insulating state at low temperatures

Keeping in mind that, strictly speaking, the standard DFT+U approach is not applicable to the IL nickelates, let us nevertheless note that all the three DFT codes are consistent in that they find a strongly dispersive electron pocket band and a much flatter hole pocket band at physically reasonable U values around 6 eV. Furthermore, the number of charge carriers occupying these electron and hole pockets is extremely small. In the specific case of the WIEN2k solution with $U = 6$ eV (Fig. 5), we find that this number corresponds to a charge carrier concentration of only 0.031 electrons and holes per formula unit. This is a situation where we have a diluted nearly-free-electron-like gas of electrons interacting with an equally diluted pool of holes that are however much more localized and residing primarily on Ni $3d$ orbitals. At low enough temperatures, such a system will have a strong

tendency to form spatially bound excitonic pairs, which, since the number of electrons and holes has to be equal because of the charge neutrality condition, can possibly result in an excitonic insulating ground state for the parent IL nickelates of the kind similar to that observed in some transition metal dichalcogenides⁷². This scenario, which is in line with the Kondo-like physics in the limit of the Nozieres exhaustion principle considered in Refs. 73 and 74, would naturally explain the measured resistivity up-turn. Also, in light of this, it is not impossible that the low-energy dispersive excitations seen in the recent RIXS measurements^{15,16} are of an excitonic origin rather than being driven by short-range magnetic order excitations.

V. CONCLUSION

In conclusion, the present study elucidates the electrone-like nature of the IL nickelates and reestablishes that in these materials “Ni⁺ is not Cu²⁺” but rather in a state closer to Ni²⁺ with substantial $d_{x^2-y^2, z^2}^{8, S=1}$ and $d_{z^2}^9 \underline{L}_{x^2-y^2}$ s contributions, in addition to the cuprate-like $d_{x^2-y^2}^9$ and $d^{10} \underline{L}_{x^2-y^2}$ ones. This results from the strong attractive potential for electrons left behind by the missing O in the NdO layer leading to a considerable charge density attracted to that region in the ground state of the undoped material. We label this region of the attractive potential with a fictitious atom with zero nuclear charge (Z) and find in DFT that its lowest-energy orbital is an s symmetry orbital.

In the language of tight-binding modeling, such peculiar charge density redistribution can be described in terms of the strong hybridization of the Ni $3d_{3z^2-r^2}$ orbital with the Z s orbital and their resulting bonding/anti-bonding like splitting that pulls some of the Ni $3d_{3z^2-r^2}$ electron density into the vacancy region in the ground state. Our TB analysis indicates also that there is a strong involvement of the Nd $5d_{xy}$ and O $2p_z$ orbitals, which, however, have only an indirect effect on the Ni $3d$ electronic structure. We also pointed out that all the theoretical methods considered so far, like DFT, the impurity calculations, and DMFT, lead to the conclusion that the d^8 states involved in the ground state are in a triplet configuration and the total configuration has spin 1/2 per formula unit. However, the propagation of this spin 1/2 composite object is much more complicated than that presented by the corresponding spin 1/2 composite object in the cuprates, which only involves the $x^2 - y^2$ holes of Cu $3d$ and a linear combination of O $2p$ orbitals of the same symmetry. Such distinct difference in the electronic behaviors of the nickelates and the cuprates is further emphasized in our calculations of their electron localization functions, which is a well documented measure of the electrone characteristics.

Our study strongly suggests that the Z s -Ni $3d_{3z^2-r^2}$ covalent bonding is a necessary component to be explicitly considered in both electronic structure and model

calculations that might eventually help us unravel the nickelates’ elusive Fermi surface as well as understand the striking sensitivity of their superconducting properties to hydrogen content. In the latter regard, we argued that if the O vacancy orbital is compensated by H⁻ as recently suggested¹⁷, this would tend to remove the need for the Ni $3d_{3z^2-r^2}$ hybridization with the Z s state to develop a negative charge in the O vacancy position and so the system would tend to be much more similar to the cuprate case. This suggests that perhaps the resulting superconductivity by the substitution of Nd with divalent Sr and with the substantial vacancy compensation by H⁻ would indeed be very similar to that of the cuprates driven mainly by the Ni $3d_{x^2-y^2}$ orbitals.

Going back to the undoped parent compound though, we also argued that because of the condition of charge neutrality of the unit cell and the material as a whole in the ground state the much discussed electron pocket is perfectly compensated by a hole pocket of equal size but occurring in the bands of mainly Ni $3d_{x^2-y^2}$ or $3d_{3z^2-r^2}$ character. This, in addition to the missing d electron charge in the Ni⁺ formal configuration, means that we must have a finite density of Ni d^8 states, be it with two holes in the $x^2 - y^2$ orbital, which would have to form a singlet as in the Zhang-Rice scenario, or with one hole in the $x^2 - y^2$ and one hole in the $3z^2 - r^2$ orbital, which locally would form an energetically favourable triplet state but for charge neutrality reasons there must also be another electron around, *i. e.*, Z s , which we find has spin opposite to the d^8 triplet so the net spin is again 1/2.

Concerning the relative likelihoods of the singlet versus triplet scenarios, a Lifschitz like transition from a Fermi surface hole pocket of the $x^2 - y^2$ symmetry into that of the $3z^2 - r^2$ symmetry is found to occur as a function of U for U values larger than 4 eV in the DFT+ U method and using Wien2k. This is, however, where we also observed significant qualitative inconsistencies between different DFT codes, such as Wien2k, VASP, and Quantum Espresso, which can be traced down to the complications that the DFT+ U method faces in the presence of a strong hybridization of correlated orbitals with their uncorrelated surroundings, which in the present case is exactly the hybridization between the interstitial Z s and Ni $3d_{3z^2-r^2}$ orbitals.

We also pointed out that the increased charge density at the oxygen vacancy position relative to the usually found rather uniform electron density in the interstitial region can be described in a DFT calculation in several different ways depending on the basis set of wave functions used. In the end, as density functional theory dictates it is only the electron density that matters. So, the extra density in the Z region can also be obtained by introducing for example $4d$ orbitals in the Ni atomic basis, which have a radial node and have their maximum amplitude in the vicinity of the O vacancy. It is the choice of the basis set and the nature of the projections in determining the state that one wants to apply U to that causes the difference in the Fermi surface for the various

codes when applying U . Although beyond the scope of this work, these observations hopefully will stimulate a more careful look at what causes this strong code dependent Fermi surface in the DFT+ U methods.

From the experimental point of view, it would be of great interest to have a detailed study of the magnetic field and temperature dependent magnetic susceptibility done using either x-ray magnetic circular dichroism spectroscopy or neutron scattering in order to gain insight into the magnetic properties of the IL nickelates. With regard to the Fermi surface, an angle-resolved photoemission spectroscopy study on high-quality stoichiometric crystals would be essential and could in principle

at least distinguish between the $x^2 - y^2$ and $3z^2 - r^2$ character at the Fermi level in the doped materials.

Acknowledgments

This research was undertaken thanks, in part, to funding from the Max Planck-UBC-UTokyo Center for Quantum Materials and the Canada First Research Excellence Fund, Quantum Materials and Future Technologies Program as well as from CIFAR and NSERC.

- ¹ D. Li, K. Lee, B. Y. Wang, M. Osada, S. Crossley, H. R. Lee, Y. Cui, Y. Hikita, and H. Y. Hwang, *Nature* **572**, 624 (2019).
- ² M. Osada, B. Y. Wang, K. Lee, D. Li, and H. Y. Hwang, *Phys. Rev. Materials* **4**, 121801 (2020), URL <https://link.aps.org/doi/10.1103/PhysRevMaterials.4.121801>.
- ³ S. Zeng, C. Li, L. E. Chow, Y. Cao, Z. Zhang, C. S. Tang, X. Yin, Z. S. Lim, J. Hu, P. Yang, et al., *Science Advances* **8**, eabl9927 (2022), <https://www.science.org/doi/pdf/10.1126/sciadv.abl9927>, URL <https://www.science.org/doi/abs/10.1126/sciadv.abl9927>.
- ⁴ G. A. Pan, D. F. Segedin, H. LaBollita, Q. Song, E. M. Nica, B. H. Goodge, A. T. Pierce, S. Doyle, S. Novakov, D. C. Carrizales, et al., *Nat. Mater.* **21**, 160 (2022).
- ⁵ J. Bednorz and K. Müller, *Z. Physik B - Condensed Matter* **64**, 189 (1986).
- ⁶ B. Keimer, S. A. Kivelson, M. R. Norman, S. Uchida, and J. Zaanen, *Nature* **518**, 179 (2015).
- ⁷ L. E. Chow and A. Ariando, *Frontiers in Physics* **10** (2022), ISSN 2296-424X, URL <https://www.frontiersin.org/articles/10.3389/fphy.2022.834658>.
- ⁸ Y. Nomura and R. Arita, *Reports on Progress in Physics* **85**, 052501 (2022), URL <https://doi.org/10.1088/1361-6633/ac5a60>.
- ⁹ Q. Gu and H.-H. Wen, *The Innovation* **3**, 100202 (2022), ISSN 2666-6758, URL <https://www.sciencedirect.com/science/article/pii/S2666675821001272>.
- ¹⁰ X. Zhou, P. Qin, Z. Feng, H. Yan, X. Wang, H. Chen, Z. Meng, and Z. Liu, *Materials Today* **55**, 170 (2022), ISSN 1369-7021, URL <https://www.sciencedirect.com/science/article/pii/S1369702122000591>.
- ¹¹ A. Botana, F. Bernardini, and A. Cano, *J. Exp. Theor. Phys.* **132**, 618 (2021).
- ¹² J. Fowlie, M. Hadjimichael, M. M. Martins, D. Li, M. Osada, B. Y. Wang, K. Lee, Y. Lee, Z. Salman, T. Prokscha, et al., *Nat. Phys.* (2022).
- ¹³ R. A. Ortiz, P. Puphal, M. Klett, F. Hotz, R. K. Kremer, H. Trepka, M. Hemmida, H.-A. K. von Nidda, M. Isobe, R. Khasanov, et al., *Phys. Rev. Research* **4**, 023093 (2022), URL <https://link.aps.org/doi/10.1103/PhysRevResearch.4.023093>.
- ¹⁴ X. Zhou, X. Zhang, J. Yi, P. Qin, Z. Feng, P. Jiang, Z. Zhong, H. Yan, X. Wang, H. Chen, et al., *Advanced Materials* **34**, 2106117 (2022), <https://onlinelibrary.wiley.com/doi/pdf/10.1002/adma.202106117>, URL <https://onlinelibrary.wiley.com/doi/abs/10.1002/adma.202106117>.
- ¹⁵ H. Lu, M. Rossi, A. Nag, M. Osada, D. F. Li, K. Lee, B. Y. Wang, M. Garcia-Fernandez, S. Agrestini, Z. X. Shen, et al., *Science* **373**, 213 (2021), <https://www.science.org/doi/pdf/10.1126/science.abd7726>, URL <https://www.science.org/doi/abs/10.1126/science.abd7726>.
- ¹⁶ M. Rossi, M. Osada, J. Choi, S. Agrestini, D. Jost, Y. Lee, H. Lu, B. Y. Wang, K. Lee, A. Nag, et al., *A broken translational symmetry state in an infinite-layer nickelate* (2021), URL <https://arxiv.org/abs/2112.02484>.
- ¹⁷ X. Ding, C. C. Tam, X. Sui, Y. Zhao, M. Xu, J. Choi, H. Leng, J. Zhang, M. Wu, H. Xiao, et al., *Nature* **615**, 50 (2023).
- ¹⁸ K.-W. Lee and W. E. Pickett, *Phys. Rev. B* **70**, 165109 (2004), URL <https://link.aps.org/doi/10.1103/PhysRevB.70.165109>.
- ¹⁹ M. Jiang, M. Berciu, and G. A. Sawatzky, *Phys. Rev. Lett.* **124**, 207004 (2020), URL <https://link.aps.org/doi/10.1103/PhysRevLett.124.207004>.
- ²⁰ J. Zaanen, G. A. Sawatzky, and J. W. Allen, *Phys. Rev. Lett.* **55**, 418 (1985), URL <https://link.aps.org/doi/10.1103/PhysRevLett.55.418>.
- ²¹ E. Been, W.-S. Lee, H. Y. Hwang, Y. Cui, J. Zaanen, T. Devereaux, B. Moritz, and C. Jia, *Phys. Rev. X* **11**, 011050 (2021), URL <https://link.aps.org/doi/10.1103/PhysRevX.11.011050>.
- ²² M. Rossi, H. Lu, A. Nag, D. Li, M. Osada, K. Lee, B. Y. Wang, S. Agrestini, M. Garcia-Fernandez, J. J. Kas, et al., *Phys. Rev. B* **104**, L220505 (2021), URL <https://link.aps.org/doi/10.1103/PhysRevB.104.L220505>.
- ²³ Y. Zhang, Z. Xiao, T. Kamiya, and H. Hosono, *The Journal of Physical Chemistry Letters* **6**, 4966 (2015), pMID: 26618554, <https://doi.org/10.1021/acs.jpcllett.5b02283>, URL <https://doi.org/10.1021/acs.jpcllett.5b02283>.
- ²⁴ S. Matsuishi, Y. Toda, M. Miyakawa, K. Hayashi, T. Kamiya, M. Hirano, I. Tanaka, and H. Hosono, *Science* **301**, 626 (2003), <https://www.science.org/doi/pdf/10.1126/science.1083842>, URL <https://www.science.org/doi/abs/10.1126/science.1083842>.
- ²⁵ C. Liu, S. A. Nikolaev, W. Ren, and L. A. Burton, J.

- Mater. Chem. C **8**, 10551 (2020), URL <http://dx.doi.org/10.1039/D0TC01165G>.
- ²⁶ Y. Zhang, B. Wang, Z. Xiao, Y. Lu, T. Kamiya, Y. Uwatoko, H. Kageyama, and H. Hosono, npj Quant Mater **2**, 45 (2017).
- ²⁷ H. W. A. M. Rompa, M. F. H. Schuurmans, and F. Williams, Phys. Rev. Lett. **52**, 675 (1984), URL <https://link.aps.org/doi/10.1103/PhysRevLett.52.675>.
- ²⁸ S. G. Dale and E. R. Johnson, The Journal of Physical Chemistry A **122**, 9371 (2018), pMID: 30339025, <https://doi.org/10.1021/acs.jpca.8b08548>, URL <https://doi.org/10.1021/acs.jpca.8b08548>.
- ²⁹ M.-s. Miao and R. Hoffmann, Journal of the American Chemical Society **137**, 3631 (2015), pMID: 25706033, <https://doi.org/10.1021/jacs.5b00242>, URL <https://doi.org/10.1021/jacs.5b00242>.
- ³⁰ F. C. Zhang and T. M. Rice, Physical Review B **37**, 3759 (1988).
- ³¹ M. Jiang, M. Berciu, and G. A. Sawatzky, Physical Review B **106**, 115150 (2022).
- ³² P. Blaha, K. Schwarz, F. Tran, R. Laskowski, G. K. H. Madsen, and L. D. Marks, The Journal of Chemical Physics **152**, 074101 (2020), <https://doi.org/10.1063/1.5143061>, URL <https://doi.org/10.1063/1.5143061>.
- ³³ J. P. Perdew, K. Burke, and M. Ernzerhof, Phys. Rev. Lett. **77**, 3865 (1996), URL <https://link.aps.org/doi/10.1103/PhysRevLett.77.3865>.
- ³⁴ F. J. d. Santos and N. Marzari, *Fermi energy determination for advanced smearing techniques* (2022), URL <https://arxiv.org/abs/2212.07988>.
- ³⁵ G. Kresse and J. Furthmüller, Computational Materials Science **6**, 15 (1996), ISSN 0927-0256, URL <https://www.sciencedirect.com/science/article/pii/S0927025696000080>.
- ³⁶ P. Giannozzi, S. Baroni, N. Bonini, M. Calandra, R. Car, C. Cavazzoni, D. Ceresoli, G. L. Chiarotti, M. Cococcioni, I. Dabo, et al., Journal of Physics: Condensed Matter **21**, 395502 (2009), URL <https://doi.org/10.1088/0953-8984/21/39/395502>.
- ³⁷ P. Giannozzi, O. Andreussi, T. Brumme, O. Bunau, M. B. Nardelli, M. Calandra, R. Car, C. Cavazzoni, D. Ceresoli, M. Cococcioni, et al., Journal of Physics: Condensed Matter **29**, 465901 (2017), URL <https://doi.org/10.1088/1361-648x/aa8f79>.
- ³⁸ N. Marzari and D. Vanderbilt, Phys. Rev. B **56**, 12847 (1997), URL <https://link.aps.org/doi/10.1103/PhysRevB.56.12847>.
- ³⁹ G. Pizzi, V. Vitale, R. Arita, S. Blügel, F. Freimuth, G. Géranton, M. Gibertini, D. Gresch, C. Johnson, T. Koeetsune, et al., Journal of Physics: Condensed Matter **32**, 165902 (2020), URL <https://doi.org/10.1088/2F1361-648x/2Fab51ff>.
- ⁴⁰ M.-Y. Choi, W. E. Pickett, and K.-W. Lee, Phys. Rev. Research **2**, 033445 (2020), URL <https://link.aps.org/doi/10.1103/PhysRevResearch.2.033445>.
- ⁴¹ See Supplementary Material at ...
- ⁴² M. Osada, B. Y. Wang, B. H. Goodge, K. Lee, H. Yoon, K. Sakuma, D. Li, M. Miura, L. F. Kourkoutis, and H. Y. Hwang, Nano Letters **20**, 5735 (2020).
- ⁴³ M. Osada, B. Y. Wang, B. H. Goodge, S. P. Harvey, K. Lee, D. Li, L. F. Kourkoutis, and H. Y. Hwang, Advanced Materials **33** (2021).
- ⁴⁴ Y. Gu, S. Zhu, X. Wang, J. Hu, and H. Chen, Commun Phys **3**, 84 (2020).
- ⁴⁵ Y. Nomura, M. Hirayama, T. Tadano, Y. Yoshimoto, K. Nakamura, and R. Arita, Phys. Rev. B **100**, 205138 (2019), URL <https://link.aps.org/doi/10.1103/PhysRevB.100.205138>.
- ⁴⁶ T. Y. Xie, Z. Liu, C. Cao, Z. F. Wang, J. L. Yang, and W. Zhu, Physical Review B **106**, 035111 (2022).
- ⁴⁷ L. Si, W. Xiao, J. Kaufmann, J. M. Tomczak, Y. Lu, Z. Zhong, and K. Held, Physical Review Letters **124**, 166402 (2020).
- ⁴⁸ A. D. Becke and K. E. Edgecombe, J. Chem. Phys. **92**, 5397 (1990).
- ⁴⁹ A. Savin, O. Jepsen, J. Flad, O. K. Andersen, H. Preuss, and H. G. von Schnering, Angewandte Chemie International Edition in English **31**, 187 (1992), <https://onlinelibrary.wiley.com/doi/pdf/10.1002/anie.199201871>, URL <https://onlinelibrary.wiley.com/doi/abs/10.1002/anie.199201871>.
- ⁵⁰ V. M. Katukuri, N. A. Bogdanov, O. Weser, J. van den Brink, and A. Alavi, Physical Review B **102**, 241112 (2020).
- ⁵¹ J. P. Perdew, M. Ernzerhof, and K. Burke, J. Chem. Phys. **105**, 9982 (1996).
- ⁵² V. I. Anisimov, J. Zaanen, and O. K. Andersen, Phys. Rev. B **44**, 943 (1991), URL <https://link.aps.org/doi/10.1103/PhysRevB.44.943>.
- ⁵³ Z. Liu, Z. Ren, W. Zhu, Z. Wang, and J. Yang, npj Quantum Materials **5** (2020).
- ⁵⁴ M. Hepting, D. Li, C. J. Jia, H. Lu, E. Paris, Y. Tseng, X. Feng, M. Osada, E. Been, Y. Hikita, et al., Nature Materials **19**, 381–385 (2020).
- ⁵⁵ G. Trimarchi, Z. Wang, and A. Zunger, Physical Review B **97**, 035107 (2018).
- ⁵⁶ A. I. Liechtenstein, V. I. Anisimov, and J. Zaanen, Phys. Rev. B **52**, R5467 (1995), URL <https://link.aps.org/doi/10.1103/PhysRevB.52.R5467>.
- ⁵⁷ F. Lechermann, Phys. Rev. X **10**, 041002 (2020), URL <https://link.aps.org/doi/10.1103/PhysRevX.10.041002>.
- ⁵⁸ F. Lechermann, Physical Review B **101**, 081110 (2020).
- ⁵⁹ I. Leonov, S. L. Skornyakov, and S. Y. Savrasov, Physical Review B **101**, 241108 (2020).
- ⁶⁰ F. Petocchi, V. Christiansson, F. Nilsson, F. Aryasetiawan, and P. Werner, Phys. Rev. X **10**, 041047 (2020), URL <https://link.aps.org/doi/10.1103/PhysRevX.10.041047>.
- ⁶¹ Y. Wang, C.-J. Kang, H. Miao, and G. Kotliar, Phys. Rev. B **102**, 161118 (2020), URL <https://link.aps.org/doi/10.1103/PhysRevB.102.161118>.
- ⁶² W. E. Pickett, Nat Rev Phys **3**, 7 (2021).
- ⁶³ P. Werner and S. Hoshino, Phys. Rev. B **101**, 041104 (2020), URL <https://link.aps.org/doi/10.1103/PhysRevB.101.041104>.
- ⁶⁴ R. A. Ortiz, H. Menke, F. Misják, D. T. Mandadakis, K. Fürsich, E. Schierle, G. Logvenov, U. Kaiser, B. Keimer, P. Hansmann, et al., Phys. Rev. B **104**, 165137 (2021), URL <https://link.aps.org/doi/10.1103/PhysRevB.104.165137>.
- ⁶⁵ J. Karp, A. Hampel, and A. J. Millis, Phys. Rev. B **103**, 195101 (2021), URL <https://link.aps.org/doi/10.1103/PhysRevB.103.195101>.
- ⁶⁶ G. Sawatzky and R. Green, in *Quantum Materials: Experiments and Theory*, Modeling and Simulation, Vol. 6, edited by E. Pavarini, E. Koch, J. van den Brink, and G.

- Sawatzky (Forschungszentrum Jülich, Jülich, 2016) pp. 1.1 – 1.35.
- ⁶⁷ A. Sleight, J. Gillson, and P. Bierstedt, *Solid State Communications* **17**, 27 (1975), ISSN 0038-1098, URL <https://www.sciencedirect.com/science/article/pii/0038109875903270>.
- ⁶⁸ K. Foyevtsova, A. Khazraie, I. Elfimov, and G. A. Sawatzky, *Phys. Rev. B* **91**, 121114 (2015), URL <https://link.aps.org/doi/10.1103/PhysRevB.91.121114>.
- ⁶⁹ J. Goodenough, D. Wickham, and W. Croft, *Journal of Physics and Chemistry of Solids* **5**, 107 (1958), ISSN 0022-3697, URL <https://www.sciencedirect.com/science/article/pii/0022369758901367>.
- ⁷⁰ K. Foyevtsova, I. Elfimov, J. Rottler, and G. A. Sawatzky, *Phys. Rev. B* **100**, 165104 (2019), URL <https://link.aps.org/doi/10.1103/PhysRevB.100.165104>.
- ⁷¹ M. L. Medarde, *Journal of Physics: Condensed Matter* **9**, 1679 (1997), URL <https://doi.org/10.1088/0953-8984/9/8/003>.
- ⁷² J. A. Wilson, *Solid State Communications* **22**, 551 (1977).
- ⁷³ Y. feng Yang and G.-M. Zhang, *Frontiers in Physics* **9** (2022).
- ⁷⁴ T. N. Shao, Z. T. Zhang, Y. J. Qiao, Q. Zhao, H. W. Liu, X. X. Chen, W. M. Jiang, C. L. Yao, X. Y. Chen, M. H. Chen, et al. (2022).